

Response to comments of Anonymous Referees

Our responses to these two referees' comments are shown below in BLUE, with the referees' comments shown as BLACK text.

Response to comments of Anonymous Referee #1

Overall assessments:

Dear Authors

I really appreciate your efforts to improve the quality of your manuscript. Nonetheless, some parts are still not very clear to me.

RESPONSE:

Thank you for your appreciation on the quality improvement, and we are so grateful for these comments below. These comments, such as the procedure of SPI3 computation and computing μ and σ , really help me realize that the revised expression is still information-missing in some certain places. If not improved or corrected in time, they tend to be confusing and difficult to understand for potential readers. The detailed responses to these comments are listed below and relevant contents have been improved in the latest revised manuscript.

Major comments:

For instance, I still do not understand the procedure applied for computing SPI3.

Following your description, a running window of 90 days is applied to daily precipitation, so that the time unit is 1-day rather than 1-month, as in the original procedure developed by McKee et al. (1993). What is doubtful is that according to Fig.3, SPI series are, apparently, computed by first fitting a gamma function to the precipitation data from the same day within the running window, for all the years included in the historical record. The gamma distribution is then transformed into a normal distribution. In the original procedure, the precipitation totals from the same 3-month period are fitted to a probability distribution (usually gamma) and then transformed to a normal distribution, so that the SPI is referred to the last month of the considered 3-month period. In this way, SPI is designed to quantify the precipitation deficit for a 3-month timescales.

In Fig. 3, you refer to 90-day mean value. Thus, the reader is left to suppose that in SPI3 is derived by averaging daily SPI within a 90-day running period. However, this is denied in Section 3.2 and in Fig. 4, where it seems that the whole time evolution of daily SPI is considered instead. If this is correct, I suggest to improve Fig. 3 and to better clarify in Section 3.1.

RESPONSE:

Thank you for this comment very much; Otherwise, we will not realize that the original expression of Fig.3 is possible to be clear and misleading. Actually, with respect to the correct approach of SPI3 calculation, we quite agree with what you understand and the original procedure developed by McKee et al. (1993). Accordingly, the third step in the original Fig.3 is to calculate 90-day-mean precipitation data first, and then calculate SPI3 from the same day based on the computed 90-day-mean precipitation data.

For better clarity, in Fig.3 of the latest revision, "Calculating 90-day-mean precipitation

data” and “calculating SPI3 series updated daily” are shown in a sequential way, respectively. In addition, we also have replaced the original expression “For values with the same day number” with “For 90-day-mean values with the same day number” in the fourth step of the latest version.

Besides, following Section 3.2, the highest negative SPI3-grade is assigned to a drought process (i.e. when SPI3 values are below -0.50 for more than 30 consecutive days) when the corresponding duration is greater than 35% of the total drought duration. What is the rationale behind the choice of 35% threshold? Have you carried out some kind of sensitivity analysis on the threshold value?

RESPONSE:

In terms of the choice of 35% threshold, some analysis was also conducted. As shown in Figure 1 (below the text), numbers of identified severe and extreme processes generally declined with the increase of threshold percent. When the threshold percent is relatively low, a large number of severe and extreme processes with “low standard” were identified, and some of them essentially can not meet the extreme or severe criteria. However, when it comes to be no less than 45%, the figure for identified processes is relatively low and even no extreme drought processes were identified in East China and North China.

Considering these two aspects, we finally chose the 35% threshold and thought it reasonable. Due to the limitation of manuscript pages, we ignored this select procedure in the manuscript.

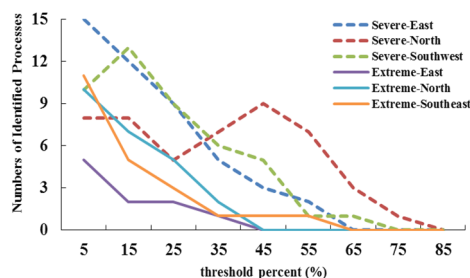


Figure 1. Relationship between numbers of identified severe and extreme processes and threshold percent in East, North and Southwest China.

With reference to Section 4 “Drought process division” and Section 5 “Predictor construction”, I evaluate the revised manuscript definitively improved. My only request of clarification is with respect to the EOF analysis applied to the atmospheric and oceanic standardized anomalies. As far as I have understood from the revised manuscript, EOF analysis is applied to SA daily grid point data of 200 hPa/500 hPa HGT and SST corresponding to the drought segments with the same dry/wet spell and drought grade (extreme or severe) according to Table 4. Therefore, μ and σ are the daily grid-point mean value and daily grid-point standard deviation computed with reference to the period indicated in Table 4 (e.g. for wet spell and extreme dry condition, μ and σ are computed on daily data observed during 21/6/1997–10/9/1997 and 4/8/1998–10/9/1998). Is it correct?

RESPONSE:

No, it is not correct. Personally, some necessary information about methods of μ and σ computation need to be specified. Without them, it may lead to being misunderstood. Therefore, we really thank you for pointing out this problem.

80 Actually, in original section 5.1, the original expression “The climatological periods are
81 1979–2008 for 200 hPa/500 hPa HGT and 1982–2008 for SST, respectively.” has
82 contained the computation methods of μ and σ . However, for more clarity, some
83 supplement has been added into section 5.1 of the latest revision, which are as follows:
84 “For example, with respect to one certain grid point, both the mean 1 January 500 hPa
85 HGT value and associated standard deviation are computed on the 1 January 500 hPa
86 HGT datasets observed during 1979–2008 at the grid point”.

87
88 With respect to Section 6.1, synchronous statistical relationship are determined between all 90-day-
89 accumulated SA-based predictors and prediction target SPI3 by using a stepwise regression. From
90 lines 637 “the predictor is area-averaged over all gridded SA-based variables in selected areas, such
91 as A and B ...”, I understand that regression (see Table 6 and Table 7) are computed only with
92 respect to the most significant positive and negative pattern areas in the first EOF, as reported in
93 Figs. 8, 9 and 10 and Table 5. If I am right, the prediction model, based on the considered predictors,
94 is performed only with reference to limited areas, rather than on the whole China, as Fig. 11 and Fig.
95 12 imply. Would you please clarify this issue?

96 RESPONSE:

97 Yes, we would. At first, thank you for this comment. Actually, regression are computed
98 only with respect to these significantly positive and negative areas in the first EOF, and
99 these anomalous areas are closely related to one prediction target region, such as North
100 China, East China or Southwest China. The original Table 6, Table 7, Figs. 8, 9 and 10
101 and Table 5 are all with respect to North China. North China, these figures and tables
102 serve, has also been involved in corresponding captions. The reason is that North China
103 was used to introduce the methods of the model construction and calibration. Due to
104 the limitation of manuscript pages, figures and tables associated with similar procedures
105 in East China and Southwest China are not shown in the present manuscript, but
106 important results of process simulation and prediction are shown and analyzed in the
107 manuscript.

108 Overall, process-based drought prediction model is applied in four recent severe
109 regional drought events in China, which are droughts in East China, North China and
110 Southwest China. Therefore, we focus on model simulation and prediction in these three
111 study regions, but only take North China as an example of methodology introduction.
112 To avoid misunderstanding, the three drought study regions we focus on are labelled
113 with red boxes in Fig.2. Besides, the word “regional” has been inserted into the title of
114 this manuscript. In addition, the last paragraph in the Introduction section has also
115 emphasized it.

116
117 Equation at line 360 (page 7) is maybe out of position.

118 RESPONSE:

119 We have made this Equation in the appropriate position.

120
121 There are still some typos in the text, such as “metrological” or “El nirio”. Please check!

122 RESPONSE:

123 We have corrected the typos in the text.

Response to comments of Anonymous Referee #2

General comment

I want to thank the authors for thoroughly taking into account the comments made by the other reviewer and myself in this revision. The changes have substantially improved the quality of the paper and now propose a clear overview of the different (and numerous) work steps presented. More specifically, I really appreciate Figures 1 and 4 as they answer many of the questions I had after reading the first manuscript.

RESPONSE:

Thank you for your appreciation about the revision. Without the advisable suggestions proposed by you and Referee #1, it is hard for us to make the manuscript clear, and easily understood.

The significant changes, which I am satisfied with, have considerably increased the length of the paper: 8 more pages in the revised version than in the original manuscript. As a general comment, I would advise authors to cut text where possible, even though I understand that it may be difficult to fit the new and relevant information into a shorter paper. Possible suggestions include: removing Figure 3, removing Figure 6 because Figure 7 and Table 4 apply in a very clear way the theoretical cases of Figure 6 to the studied drought events.

RESPONSE:

Thank you for this comment, and it is actually necessary to make it shorter. Considering the information some figures and tables expressed is helpful for potential readers to understand the procedures of model construction, we tend to move them into the Supplement part. Detailed revision and relevant reasons are as follows:

(1) We have made the original Figure 3 reserved. It explains methods of computing SPI3 updated daily, which is something new to potential readers. Referee #1 also showed its concern on it.

(2) We have made the original Figure 6 reserved, because this universal rules is valuable. Accordingly, the original Figure 7, which acts as application cases of the theoretical rules, have been moved to the Supplement part. In addition, the original Table 4 is still in its position of the manuscript.

(3) Finally, to cut text where possible, the original Figure 9 has been also moved to the Supplement part, since it is similar to the original Figure 8 but for 200 hPa HGT SA. Besides, the original Table 7 has been also moved to the Supplement part. The reason is that it contains necessary and detailed information about selected predictors and relevant coefficients, despite associated little analysis in the manuscript.

Minor comment

Lines 70-74: Point (3) and point (4) could be inverted to follow the new structure of the paper.

RESPONSE:

Thank you for this comment, and we have made them inverted.

A conceptual prediction model for seasonal drought processes using atmospheric and oceanic standardized anomalies and its application to four recent severe regional drought events in China

Zhenchen Liu¹, Guihua Lu¹, Hai He¹, Zhiyong Wu¹, Jian He²

¹ College of Hydrology and Water Resources, Hohai University, Nanjing, China.
² Hydrology and Water Resources Investigation Bureau of Jiangsu Province, Nanjing, China.
Correspondence to: Hai He (hehai_hhu@hhu.edu.cn)

Abstract. Reliable drought prediction is fundamental for water resource managers to develop and implement drought mitigation measures. Considering that drought development is closely related to the spatio-temporal evolution of large-scale circulation patterns, we develop a conceptual prediction model of seasonal drought processes based on atmospheric/oceanic Standardized Anomalies (SA). Empirical Orthogonal Function (EOF) analysis is first applied to drought-related SA at 200 hPa/500 hPa geo-potential height (HGT) and sea surface temperature (SST). Subsequently, SA-based predictors are built based on the spatial pattern of the first EOF modes. This drought prediction model is essentially the synchronous statistical relationship between 90-day-accumulated atmospheric/oceanic SA-based predictors and 3-month SPI (SPI3), calibrated using a simple stepwise regression method. It is forced with seasonal climate forecast systems, including the NCEP Climate Forecast System Version 2 (CFSv2). It can make seamless drought prediction for operational use after a year-to-year calibration. Model application to four recent severe regional drought events in China indicates its good performance in predicting seasonal drought development, despite its weakness in predicting drought severity. Therefore, it can provide some valuable information and is a worthy reference for seasonal water resource management.

1 Introduction

Drought is an economically and ecologically disruptive natural hazard that profoundly impacts water resources, agriculture, ecosystems, and basic human welfare (Dai, 2011). In recent years, extreme drought events have caused disastrous impacts worldwide. The 2011 East Africa drought led to famine and severe food crises in several countries, affecting over nine million people (Funk, 2011). As part of the 2011–14 California Drought, the drought in 2014 alone cost California \$2.2 billion in damages and 17000 agricultural jobs (Howitt et al., 2014). China has also suffered from extreme drought events, such as the 2009/2010 severe drought in Southwest China (Yang et al., 2012), 2011 spring drought in the Yangtze River basin (Lu et al., 2014), and 2014 summer drought in North China (Wang and He, 2015). Because drought is a costly and disruptive natural hazard, reliable drought prediction is fundamental for water resource managers to develop and implement feasible drought

删除的内容: Standardized Anomalies

删除的内容: models

mitigation measures. In the present study, drought prediction is restricted to meteorological drought, which is associated with long-term precipitation deficits.

Drought is generally predicted using two types of methods: model-based dynamical forecasting and statistical prediction.

35 Dynamical forecasting primarily relies on computed drought indicators, such as the Standardized Precipitation Index (SPI; McKee and Kleist, 1993), based on forecasted precipitation retrieved from seasonal climate forecast [systems](#) (Dutra et al., 2013; Dutra et al., 2014; Mo and Lyon, 2015; Yoon et al., 2012). Although dynamically predicted precipitation is useful information for drought situations, especially for short-term forecasting, it also contains high levels of uncertainty and limited skill with respect to long lead times (Wood et al., 2015; Yoon et al., 2012; Yuan et al., 2013). In contrast, statistical drought
40 prediction is an additional source of prospective drought information (Behrangi et al., 2015; Hao et al., 2014). Different from the physically complex processes in coupled atmosphere-ocean models used for dynamical prediction, statistical drought prediction models are relatively simple but also perform well. They consist of input variables, methodology, and prediction targets (Mishra and Singh, 2011).

Reasons for good and effective performance of statistical models include methodology improvements and drought-related
45 climate indices used as input variables. To date, much attention has been paid to methodology improvements. Taking advantage of probabilistic and temporal-evolution features of input variables, statistical drought prediction models are primarily forced with probability or machine-learning methods, such as the ensemble streamflow prediction (ESP) method (AghaKouchak, 2014), Markov Chain- and Bayesian Network-Based Models (Aviles et al., 2015; Aviles et al., 2016; Shin et al., 2016), neural network, and support vector models (Belayneh et al., 2014). In addition to method improvement, climate indices represent
50 large-scale atmospheric or oceanic drivers of precipitation, partly responsible for effective model performance. These climate indices include typical atmospheric and oceanic circulation patterns, such as the North Atlantic Oscillation (NAO; Hurrell, 1995) and El Niño-Southern Oscillation (ENSO; Ropelewski and Halpert, 1987), which have been widely used for drought prediction in different seasons and regions (Behrangi et al., 2015; Bonaccorso et al., 2015; Chen et al., 2013; Mehr et al., 2014; Moreira et al., 2016).

55 These inherent climate indices, such as the NAO index and NINO 3.4 index, are simple, explicit, and widely used, therefore, they are the primary indices used for drought prediction. Additionally, based on the relationship between drought indices and potential atmospheric or oceanic circulation patterns, some [researchers](#) have also discovered large-scale circulation patterns closely related to regional droughts or have structured new drought predictors (Funk et al., 2014; Kingston et al., 2015). For instance, after discovering the two dominant modes of the East African boreal spring rainfall variability that are tied to SST
60 fluctuations, Funk et al. (2014) further determined that the first- and second-mode SST correlation structures were related to two SST indices that could be used to predict East African spring droughts.

Similarly, potential atmospheric and oceanic circulation patterns, which are closely related to regional droughts, are also used to construct drought predictors in the present study. Considering that the development of drought processes is closely related to the spatio-temporal evolution of large-scale circulation patterns, we constructed predictors based on anomalous spatial
65 patterns. Because precipitation-inducing circulation patterns usually occur in the troposphere, predictors can be built based on

删除的内容: models

删除的内容: researchers

sea surface temperature (SST) and 200 hPa/500 hPa geopotential height (HGT), reflecting information from different levels of the troposphere. Subsequently, all predictors during different drought processes and 3-month SPI updated daily (hereafter SPI3) were used to calibrate the synchronous stepwise-regression relationship. The model can be forced with dynamically predicted SST and 200 hPa/500 hPa HGT conditions, indicating that the lead-time depends on that of the climate forecast models. Based on predicted prospective 90-day SPI3 curves, we developed angle-based rules for the drought outlook, which can make the drought outlook easily accessible to water resource managers.

Overall, the objective of this study is to build a conceptual prediction model of seasonal drought processes. The essential and important steps are to (1) structure predictors on the basis of drought-related atmospheric/oceanic circulation patterns; (2) build the synchronous statistical predictor-SPI3 relationship forced with reanalysis and operationally forecasted datasets; (3) simulate and predict four severe seasonal drought processes in China to investigate model performance; and (4) propose an objective angle-based method for drought outlook.

Considering the proposed conceptual model consists of several important parts, a brief but general introduction with sequential procedures are shown (Fig. 1), prior to specific descriptions in Sect. 3 to Sect. 8. In Sect. 3, historical extreme and severe drought processes are identified with 3-month SPI updated daily (SPI3). These drought processes usually go through one or several dry/wet spells, in which precipitation deficit characteristics and circulation patterns vary. Therefore, process-split rules according to dry/wet spells in Sect. 4 are designed to assign drought process segments to different dry/wet spells. Meanwhile, gridded values in the fields of 200 hPa/500 hPa HGT and SST are transformed into gridded values of Standardized Anomalies (SA) in Sect. 5. Maps of atmospheric/oceanic SA during drought process segments within the same dry/wet spells are important inputs of predictor construction. After Empirical Orthogonal Function (EOF) analyses are conducted on these SA-based maps, the first leading EOF modes are used to generate predictors (Sect. 5). Further, synchronous statistical relationships between SA-based predictors and SPI3 are calibrated with the stepwise regression method in Sect. 6. The National Centers for Environmental Prediction / National Center for Atmospheric Research (NCEP/NCAR) Reanalysis datasets and NCEP Climate Forecast System Version 2 (CFSv2) operationally forecasted datasets are used to force the synchronous statistical relationship, respectively. Simulated and predicted 90-day prospective SPI3 time series are presented in Sect. 7. With the aid of angle-based rules for seasonal drought outlook, simulated and predicted SPI3 time series are transformed to five types of drought outlooks, which are easily accessible to water resource managers.

删除的内容: prediction

删除的内容: propose an objective angle-based method for drought outlook; and (4)

删除的内容: .

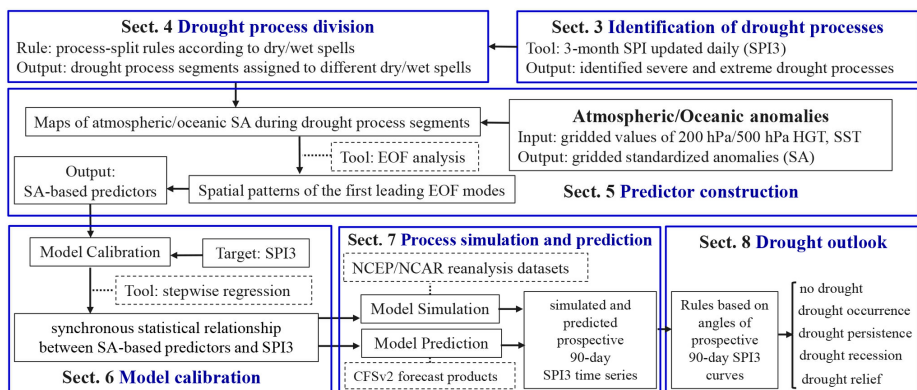


Figure 1. Brief introduction of the sequential procedures for drought prediction model construction

Additionally, historical drought events in North China were used to introduce the model construction and calibration in Sect. 3–6, but similar detailed procedures in East and Southwest China were not shown in the present study. Besides, SPI3 time series during the period extending from 2009 to 2014 in North China, East China, and Southwest China were used in the process simulation. Finally, recent severe drought processes in these three regions were used to verify model performance in operational application.

删除的内容: 3–6.

2 Data

The precipitation data used were the second-version Dataset of Observed Daily Precipitation Amounts at each $0.5^\circ \times 0.5^\circ$ grid point in China for 1961–2014 (http://data.cma.cn/data/detail/dataCode/SURF_CLI_CHN_PRE_DAY_GRID_0.5.html), which was kindly provided by the Climate Data Center (CDC) of the National Meteorological Information Center, China Meteorological Administration (CMA). It was initially used to calculate area-averaged precipitation in North China, East China, and Southwest China (Fig. 2), which are the three Chinese drought regions investigated in this study. Atmospheric anomalies were diagnosed with respect to the NCEP/NCAR Reanalysis datasets, which has a resolution of $2.5^\circ \times 2.5^\circ$ at 17 pressure levels, extending from January 1948 to the present (Kalnay et al., 1996). The National Oceanic and Atmospheric Administration (NOAA) High Resolution SST dataset, with a spatial resolution of $0.25^\circ \times 0.25^\circ$ and extends from September 1981 to present (Reynolds et al., 2007), were used for SST anomaly analysis. Additionally, the NCEP Climate Forecast System Version 2 (CFSv2; Saha et al., 2014) was introduced to verify operational performance of the proposed conceptual model. Since CFSv2 began on 1 April 2011, some drought events that occurred before this date were forced with the CFS reforecast output. All the reforecast and forecasted datasets are accessible on the website

删除的内容: and SPI3

120 (https://nomads.ncdc.noaa.gov/modeldata/), and 6-hourly forecasted datasets are transformed to daily timescale by a simple time-weighted mean method.

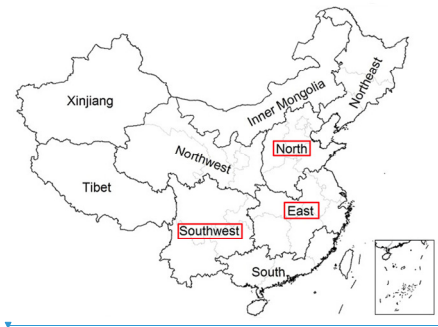


Figure 2. The geographical distribution of China's nine drought study regions (black solid curves) and provinces (light grey curves). The three regions labelled with red boxes are the focus in the present study.

125 **3 Identification of drought processes**

3.1 Three-month SPI updated daily

SPI3 was used as the drought index for seasonal drought recognition and prediction in this study, and the calculation period is 1979–2014. Traditionally, the SPI3 set varies with a monthly timescale; each month a new value was determined from the previous 3 months (McKee and Kleist, 1993). To obtain seasonal drought processes at the 1-day timescale, we chose to update SPI3 daily, which was also recommended by the World Meteorological Organization (2012). Compared with the traditional method, the essential difference is that the interval for SPI3 calculation has been extended from 1 month to 1 day. However, no other changes relevant to mathematic procedures occur. Specified illustrations and details for calculating SPI3 updated daily are shown as Fig. 3. Prior to the detailed procedures shown in Fig.3, daily area-averaged precipitation datasets are computed first.

删除的内容: /).



删除的内容:

删除的内容: Metrological

删除的内容: occur

删除的内容: 3

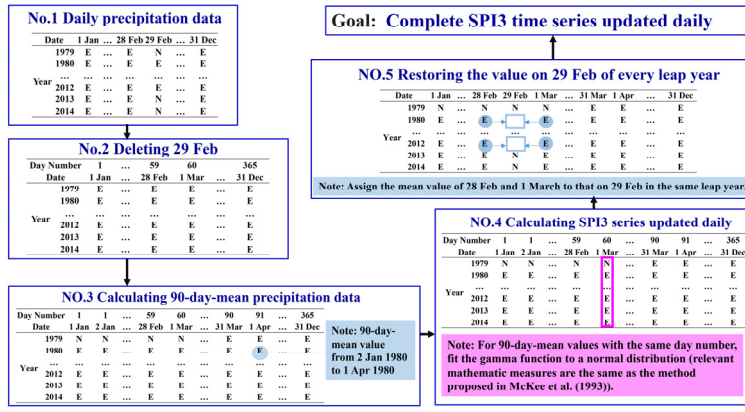


Figure 3. Illustration indicating the steps for calculating SPI3 updated daily. The letter “E” represents value existence, while the letter “N” represents no relevant data.

3.2 Drought process identification and grade classification

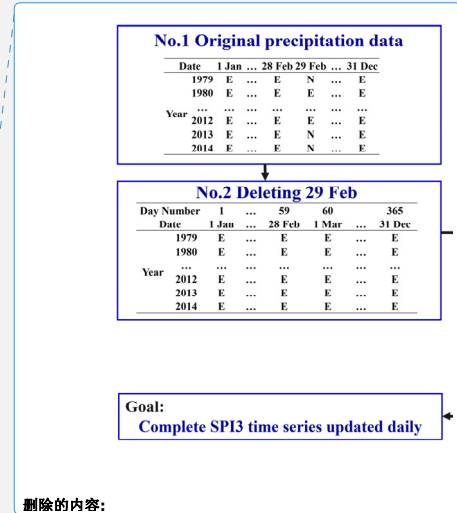
Similar to the rules for SPI grade division recommended by the World Meteorological Organization (2012), the rules in our study are shown in Table 1. Drought processes are identified when the daily SPI3 values are below -0.50 for more than 30 consecutive days.

Table 1. Rules for SPI3 grade classification.

daily SPI3 value	grade
0.50 and more	wet
-0.49 to 0.49	near normal
-0.99 to -0.50	slightly dry
-1.49 to -1.00	moderately dry
-1.99 to -1.50	severely dry
-2.00 and less	extremely dry

Each daily SPI3 value for a recognized drought process was assigned to the corresponding SPI3 grade (e.g., severely dry).

Starting from the extremely dry grade to slightly dry grade, the ratio between the duration of a particular SPI3 grade and the total days of the entire drought process is calculated. When the ratio increases beyond 35%, the corresponding grade is assigned to the entire drought process. For example, as shown in Fig. 4, the proportion of the severely dry days is beyond 35%. Accordingly, the 2001 summer drought in North China corresponded to the severe grade.



删除的内容:

删除的内容: Metrological

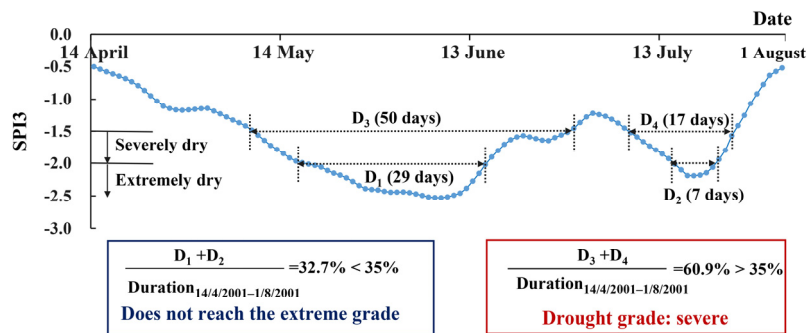


Figure 4. An example of grade classification for one complete drought process: the 2001 summer drought in North China.

Therefore, we identified severe and extreme drought processes for 1979–2008 in North China. As shown in Table 2, persistent drought periods from 1997 to 2002 in North China were found, in agreement with other associated studies (Rong et al., 2008; Wei et al., 2004).

Table 2. Identified severe and extreme drought processes from 1979 to 2008 in North China.

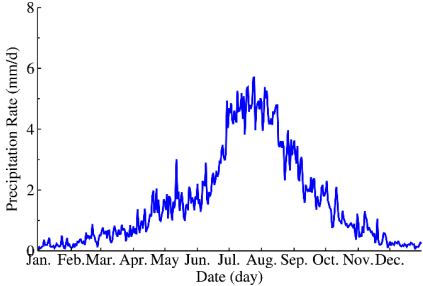
Extreme Drought	12/6/1997–28/11/1997
	2/11/1998–11/4/1999
Severe Drought	15/1/1984–14/5/1984
	9/11/1988–9/1/1989
	17/7/1999–1/11/1999
	23/3/2000–27/6/2000
	14/4/2001–1/8/2001
	3/8/2002–4/12/2002
	26/12/2005–2/2/2006

4 Drought process division according to dry/wet spells

Identified drought processes usually go through one or several dry/wet spells. Different dry/wet spells usually correspond to various precipitation deficit characteristics and atmospheric/oceanic circulation patterns. Therefore, we divided drought processes into different segments according to dry/wet spells, to further analyse atmospheric/oceanic anomalies during drought segments within the same dry/wet spells. Additionally, SPI3 on the start date also indicates that SPI3 is initially less than -0.5 and a severe drought process indeed follows, which is also important and special. Due to its implication, SPI3 on the start date

of an identified drought process actually reflects drought-inducing precipitation information for the previous 90 days. Therefore, the start date of the drought process is advanced to the past 90th day, preceding the drought process division. This measure can contribute to introducing early drought-inducing information to predictor construction.

175 Using North China as an example, the specified procedures for the division process are as follows. Similar to general seasonal classification, we divided the annual period into four dry/wet spells (Table 3) according to the temporal evolution of the daily precipitation rate in North China (Fig. 5). It is evident that the wet spell (one-fourth of the annual duration) accounts for over 50% of total precipitation, while the dry spell (one-third of the annual duration) accounts for about 6%.



180 **Figure 5.** Temporal evolution of daily precipitation rate in North China averaged from 1961 to 2010.

Table 3. Dates of dry/wet spells and their associated proportions of annual total precipitation in North China. Both Wet–Dry and Dry–Wet represent corresponding transition spells.

Spell	Period	Precipitation Proportion (%)
Wet	21 June–10 September	56.4
Wet–Dry	11 September–20 November	14.9
Dry	21 November–20 March	6.3
Dry–Wet	21 March–20 June	22.4

185 Based on these dry/wet spells, process-split rules (Fig. 6) are constructed using the Intersection Proportion (IP) and critical Proportion (P, set as 40%). Herein, IP is the proportion of initial segments accounting for relevant dry/wet spells, and the initial segments (e.g., D₁, D₃ and D₄ in Fig. 6) refer to parts of one drought process split with dry/wet spells. As shown in Fig. 6, one complete process is first transformed into several initial segments according to dry/wet spells. Second, “IP[0]” and “IP[-1]” are calculated, which express IP at the start and end segments respectively. Third, based on a comparison of IP and P results,
 190 these initial segments can be assigned to different dry/wet spells.

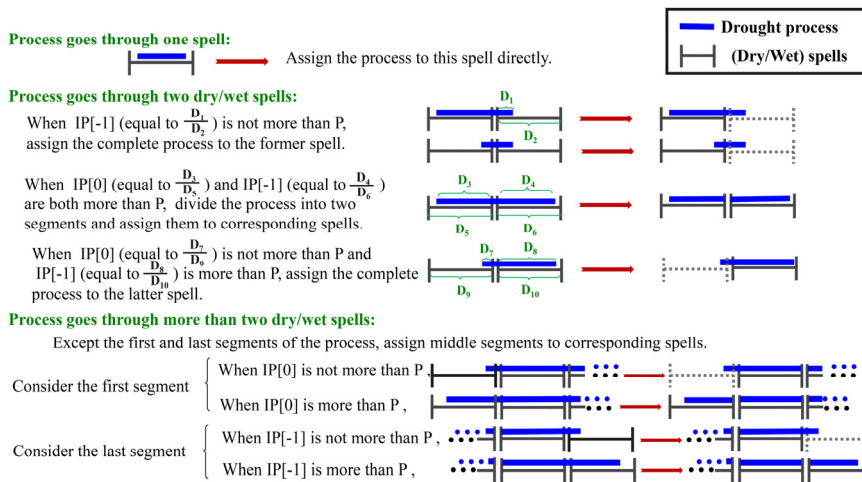


Figure 6. Process-split rules for one drought process according to dry/wet spells. IP represents Intersection Proportion, while P refers to critical Proportion. The terms “ $IP[0]$ ” and “ $IP[-1]$ ” express the IP at the start and end segments respectively.

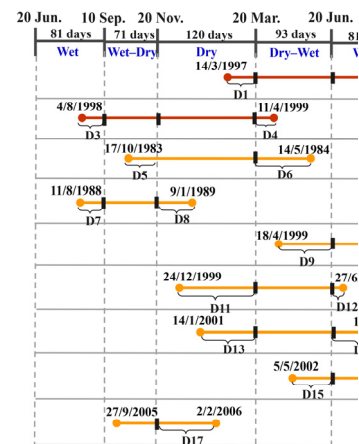
In practice, the start dates of identified drought processes (Table 2) were first shifted 90 days in advance. Following the process-split rules shown in Fig. 6, we divided these drought processes according to dry/wet spells in North China (Table 3). Detailed procedures of relevant IP calculations and comparisons can be found in Fig. S1, while final assignments of initial drought segments are shown in Table 4. In addition, to highlight the importance of extreme droughts, severe and extreme drought segments are considered respectively.

Table 4. Drought process segments assigned to dry/wet spells during 1979–2008 in North China.

Drought Grades	Dry Spell	Dry–Wet Spell	Wet Spell	Wet–Dry Spell
Extreme	21/11/1998–11/4/1999	14/3/1997–20/6/1997	21/6/1997–10/9/1997	11/9/1997–28/11/1997
	-	-	4/8/1998–10/9/1998	11/9/1998–20/11/1998
	21/11/1983–20/3/1984	21/3/1984–14/5/1984	21/6/1999–10/9/1999	17/10/1983–20/11/1983
Severe	21/11/1988–9/1/1989	18/4/1999–20/6/1999	21/6/2001–1/8/2001	11/8/1988–20/11/1988
	24/12/1999–20/3/2000	21/3/2000–27/6/2000	21/6/2002–10/9/2002	11/9/1999–1/11/1999
	14/1/2001–20/3/2001	21/3/2001–20/6/2001	-	11/9/2002–4/12/2002
	21/11/2005–2/2/2006	5/5/2002–20/6/2002	-	27/9/2005–20/11/2005

删除的内容: Relevant

删除的内容: 7



删除的内容: Figure 7. Comparison results of P , “ $IP[0]$ ” and “ $IP[-1]$ ” for drought processes during 1979–2008 in North China. The start dates of these drought processes have been shifted 90 days in advance. IP represents Intersection Proportion, while P refers to critical Proportion. The terms “ $IP[0]$ ” and “ $IP[-1]$ ” express IP of the start and end segments, respectively. .

5 Predictor construction

5.1 Atmospheric and oceanic standardized anomalies

To describe atmospheric and oceanic anomalies objectively, we chose the Standardized Anomalies (SA) method. It was first used to effectively identify high-impact weather events (Grumm and Hart, 2001; Hart and Grumm, 2001). Subsequently, the SA method has also provided significant values for the analysis of extreme precipitation events (Duan et al., 2014; Jiang et al., 2016). In the present study, the SA of a meteorological variable was defined in Hart and Grumm (2001), described as

SA = (X - μ) / σ, (1)

Where X represents daily grid-point atmospheric/oceanic circulation pattern variables, which are 200 hPa/500 hPa HGT and SST. μ and σ are the daily grid-point mean value and daily grid-point standard deviation, respectively. The climatological periods are 1979–2008 for 200 hPa/500 hPa HGT and 1982–2008 for SST, respectively. For example, with respect to one certain grid point, both the mean 1 January 500 hPa HGT values and associated standard deviation are computed on the 1 January 500 hPa HGT datasets observed during 1979–2008 at the grid point.

5.2 The first EOF leading modes of SA

Empirical Orthogonal Function (EOF) analysis (Wilks, 2011) is introduced to decompose spatio-temporal dataset of drought-related atmospheric/oceanic SA into spatially stationary coefficients (leading modes) and time-varying coefficients (principal component). Considering the first leading EOF modes reflect the largest fraction of drought-related atmospheric/oceanic spatial variability, we focus on them. In addition, to highlight the importance of extreme droughts, EOF analysis is conducted on atmospheric/oceanic SA during severe and extreme drought segments, respectively. With the same dry/wet spells and drought grade, SA-based maps during all drought process segments are used for EOF analysis. For example, SA-based maps of 500hPa HGT during all three severe segments in wet spells (Table 4) are analysed with the EOF method, and the first EOF lead mode is shown in Fig. 7(h). Identical EOF analysis is conducted on atmospheric/oceanic SA of 200/500 hPa HGT and SST during all four dry/wet spells. Relevant results are found in Fig. 7, Fig. S2 and Fig. 8, respectively.

带格式的：居中，缩进：首行缩进： 1.27 厘米

删除的内容：

删除的内容： 8

删除的内容： 8–10

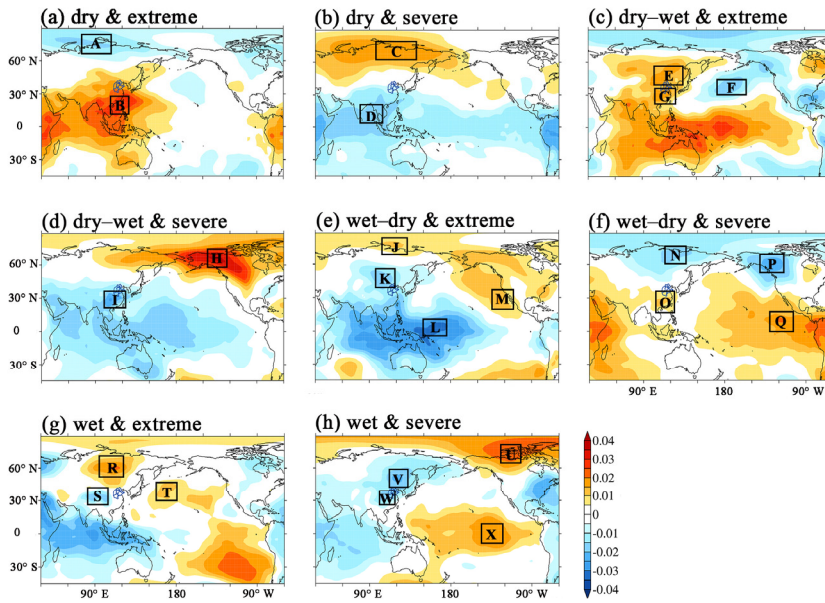


Figure 7. The first leading Empirical Orthogonal Function (EOF) modes of Standardized Anomalies (SA) for 500 hPa geo-potential height fields (HGT) during all severe and extreme drought process segments in different dry/wet spells. The black boxes outline the selected areas used to structure predictors, while capital letters refer to the selected area codes.

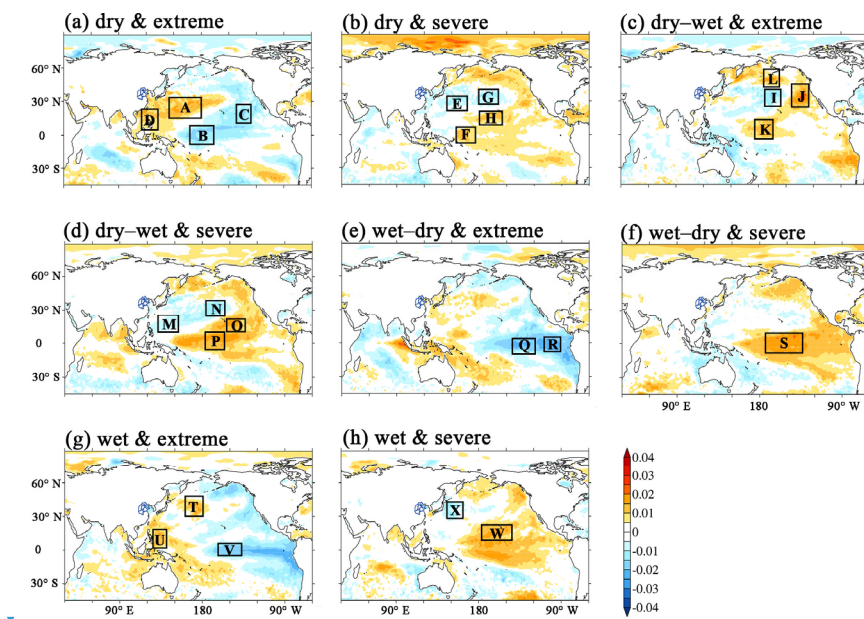
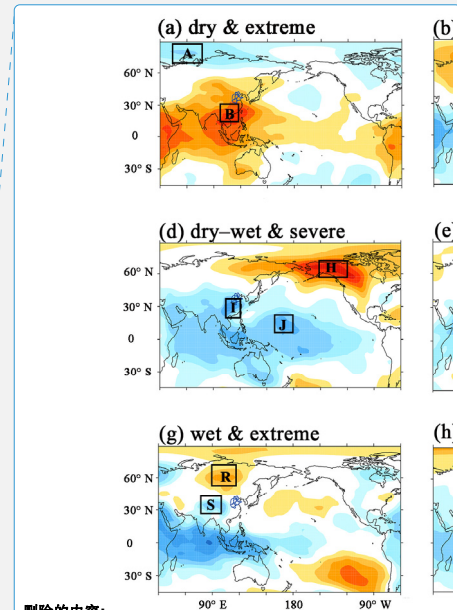


Figure 8. Same as Fig. 7, but for Standardized Anomalies (SA) of SST fields.

5.3 Pattern-based predictor construction

Positive and negative pattern areas in the first EOF leading modes are used to build predictors, which resemble the pattern-based definition of atmospheric teleconnection indices (Wallace and Gutzler, 1981). As shown in Fig. 7(a), a large area of positive pattern area (Region B) occurs over southeast China, while a negative pattern area (Region A) appears to the north of Eurasia. Generally, the predictor is area-averaged over all gridded SA-based variables in selected areas, such as A and B, considering the positive and negative signs indicated with different colours. Results from the pattern-based predictor construction are shown in Table 5.

As shown in Fig. 7, the spatial pattern of different phases in the 500 hPa HGT fields were adequately considered, including low/high latitude differences (e.g., $P_{HGT500,0}$ in Table 5) and ocean/continent differences (e.g., $P_{HGT500,3}$ in Table 5). In addition, the spatial pattern of different phases surrounding the prediction-targeted region (e.g., Region R, S and T in Fig. 7(g)) was intentionally used to construct predictors, such as $P_{HGT500,9}$ and $P_{HGT500,10}$ in Table 5. Because the first EOF modes of 200 hPa HGT (Fig. S2) were similar to those of 500 hPa HGT, the specified illustrations were ignored. Additionally, the positive and negative pattern areas in the Pacific SST SA fields were also used, especially in the subtropical gyre zone (Fig. 8 (a)–(d)) and



删除的内容:

删除的内容: 8, but for Standardized Anomalies (SA) of 200 hPa geo-potential height fields (HGT).

带格式的: 字体: +西文正文 (Times New Roman)

带格式的: 字体: +西文正文 (Times New Roman)

带格式的: 字体: +西文正文 (Times New Roman)

删除的内容: 8

带格式的: 字体: +西文正文 (Times New Roman)

删除的内容: 8

带格式的: 字体: +西文正文 (Times New Roman)

删除的内容: 8

删除的内容: 9

删除的内容: 10

El Niño region (Fig. 8 (e) and (f)). Furthermore, some regions, such as the El Niño Regions R, Q and S, were separately used for predictor construction.

Table 5. Predictor-structured results based on the first leading Empirical Orthogonal Function (EOF) modes for SA of 200 hPa HGT, 500 hPa HGT and SST fields during different dry/wet spells in North China. Capital letters refer to the code for selected areas in Fig. 7, Fig. S2 and Fig. 8. In the term “P_{XXX,Y}”, P, XXX, and Y refer to predictor, atmospheric or oceanic elements, and the code of new predictors, respectively.

Dry	Dry–Wet	Wet–Dry	Wet
P _{SST,0} =A-B	P _{SST,5} =L+K-I	P _{SST,9} =Q	P _{SST,12} =T
P _{SST,1} =D-B	P _{SST,6} =J-I	P _{SST,10} =R	P _{SST,13} =U-V
P _{SST,2} =A-C	P _{SST,7} =M-P	P _{SST,11} =S	P _{SST,14} =W-X
P _{SST,3} =F-E	P _{SST,8} =N-O	P _{HGT500,5} =J-K	P _{HGT500,9} =R-S
P _{SST,4} =H-G	P _{HGT500,2} =E-F	P _{HGT500,6} =M-L	P _{HGT500,10} =T-S
P _{HGT500,0} =B-A	P _{HGT500,3} =G-F	P _{HGT500,7} =O-N	P _{HGT500,11} =U-V
P _{HGT500,1} =C-D	P _{HGT500,4} =H-I	P _{HGT500,8} =Q-P	P _{HGT500,12} =X-W
P _{HGT200,0} =A-B	P _{HGT200,2} =F-E	P _{HGT200,6} =K-L	P _{HGT500,13} =U-W
P _{HGT200,1} =C-D	P _{HGT200,3} =F-G	P _{HGT200,7} =K-M	P _{HGT200,10} =R-S
	P _{HGT200,4} =H-I	P _{HGT200,8} =O-N	P _{HGT200,11} =X-T
-	P _{HGT200,5} =H-J	P _{HGT200,9} =Q-P	P _{HGT200,12} =V-U
	-	-	P _{HGT200,13} =W-U

6 Model calibration

6.1 Synchronous statistical relationship

Stepwise regression (Afifi and Azen, 1972) is a method for fitting multiple linear regression models, in which a predictive variable is considered for addition to or subtraction from a set of explanatory variables according to statistically significant extent or loss. It is used to build the synchronous statistical relationship between all 90-day-accumulated SA-based predictors and prediction target SPI3. SA-based predictors are calculated with the NCEP/NCAR Reanalysis dataset (Kalnay et al., 1996). Essentially, the conceptual model, aimed at seasonal drought process prediction, is a synchronous stepwise relationship.

6.2 Rolling calibration year by year

To meet the practical requirements of operational service departments, model calibration is also running year by year. Six experiments of seasonal drought prediction are conducted (Table 6). Detailed information about selected predictors and relevant coefficients can be found in Table S1. For example, the seasonal drought prediction model, calibrated from 1 Jan 1983 to 31 Dec 2011, is used for initial daily prediction time in the entire 2012 year. For every initial drought prediction in the 2013 year, the corresponding drought model is calibrated from 1 Jan 1983 to 31 Dec 2012.

删除的内容: 10

删除的内容: . .

删除的内容: 8–10.

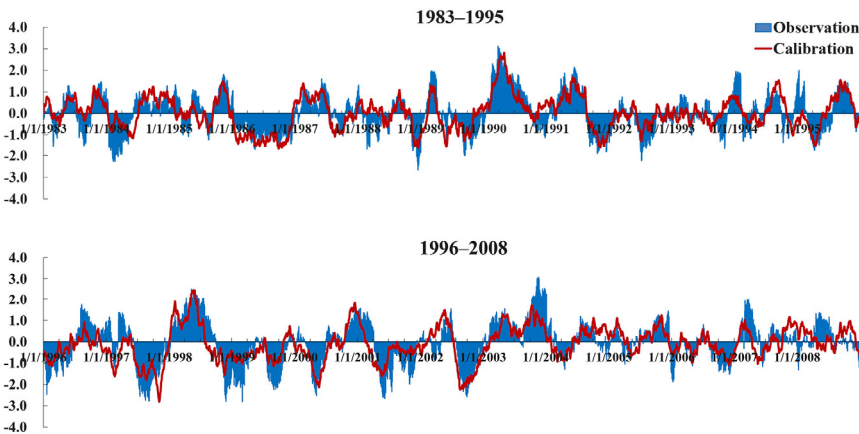
删除的内容: and 7).

带格式的: 字体颜色: 黑色

295 **Table 6.** Statistical parameters of stepwise-regression equations used for prediction during different calibration periods in North China.

Calibration period (1 Jan 1983–)	Simulation or Prediction period	Numbers of selected/initial predictors	Multiple correlation coefficient
31 Dec 2008	1 Jan 2009–31 Dec 2009	38/43	0.76
31 Dec 2009	1 Jan 2010–31 Dec 2010	37/43	0.76
31 Dec 2010	1 Jan 2011–31 Dec 2011	39/43	0.75
31 Dec 2011	1 Jan 2012–31 Dec 2012	39/43	0.76
31 Dec 2012	1 Jan 2013–31 Dec 2013	38/43	0.76
31 Dec 2013	1 Jan 2014–31 Dec 2014	39/43	0.75

300 The calibration period increases year by year, therefore, the figure for samples used for calibration is considerable. Multiple correlation coefficients in six drought prediction models are no less than 0.75. Statistical parameters and their total numbers show slight changes across the six calibration experiments (Table 6). Furthermore, calibrated SPI3 curves are almost consistent with the observation data (Fig. 9), especially with respect to the key turning points and trends.



305 **Figure 9.** Temporal evolution of observed and calibrated SPI3 during the calibration period between 1 Jan 1983 and 31 Dec 2008 in North China.

删除的内容: and Table 7

删除的内容: 11

删除的内容: Table 7. List of the selected predictors and relevant coefficients during different calibration periods in North China. Types and codes correspond to Table 5. .

Type

带格式的: 两端对齐, 定义网格后自动调整右缩进, 行距: 1.5 倍行距, 与下段不同页, 到齐到网格

.. [2]

7 Drought process simulation and prediction

7.1 Model forcing

315 Because the conceptual model is essentially a synchronous statistical relationship, the model itself has no lead time. Therefore, model simulation and prediction have to be further forced with different forecasted datasets. During the periods of model simulation, the synchronous statistical relationship is forced with the NCEP/NCAR Reanalysis dataset (Kalnay et al., 1996). For model prediction, SPI3 prediction is operationally forced with CFSv2 (Saha et al., 2014), which is a type of climate forecast model. Therefore, the lead time for the conceptual model depends on that of the climate forecast models.

320 In the present study, we focus on the prospective 90 day seasonal drought process prediction. That is, 90 daily SPI3 values in the future will be predicted and they will compose a prospective SPI3 curve with 90 points. To achieve it, prospective 90 day forecasted data subsets for 200 hPa/500 hPa HGT and SST are retrieved from CFSv2, which are used for the predictor calculation.

删除的内容: prediction
删除的内容: prediction

7.2 Drought processes simulated with the NCEP/NCAR reanalysis datasets

325 To assess model performance of severe seasonal droughts, we take recent drought events in Southwest China, East China, and North China as examples. First, Southwest China experienced two severe droughts (the black boxes in Fig. 10 (c)). Although the simulated SPI3 does not reach its peak during the 2009/2010 drought, it indicates the state transformation from drought occurrence to persistence and eventually to relief. In terms of the 2011 summer drought in the Southwest China, the simulated SPI3 indicates that the state remains wet and gradually becomes wetter, indicating no valuable information consistent with observations. Nevertheless, during the phase of drought recession, the simulated development is quite similar to the observed development. This comparison indicates that the conceptual model performs well in development but is weak in severity. This distinct feature also appears in the simulation of the 2011 drought in East China (the black box in Fig. 10 (b)) and 2014 drought in North China (the black box in Fig. 10 (a)).

带格式的: 字体: +西文正文 (Times New Roman)
删除的内容: 12
带格式的: 字体: +西文正文 (Times New Roman)
删除的内容: 12
带格式的: 字体: +西文正文 (Times New Roman)
带格式的: 字体: +西文正文 (Times New Roman)
删除的内容: 12
带格式的: 字体: +西文正文 (Times New Roman)
带格式的: 字体: +西文正文 (Times New Roman)

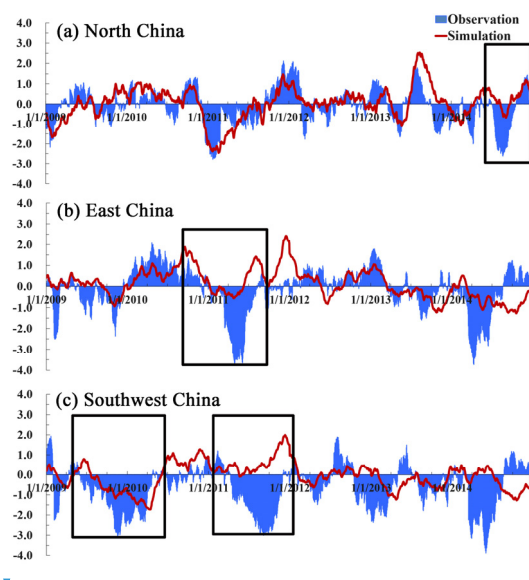
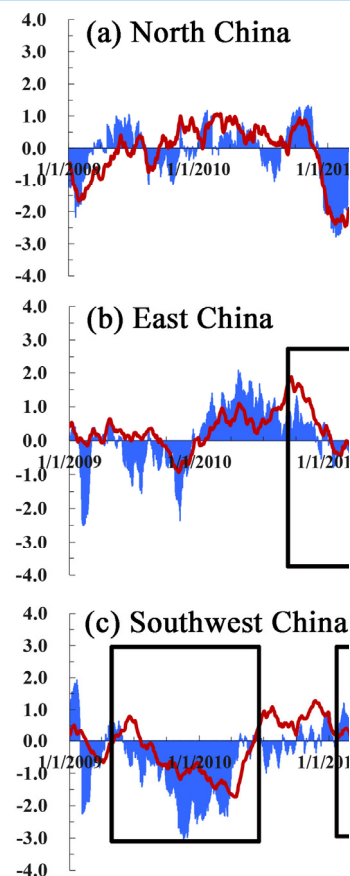


Figure 10. Temporal evolution of observed and simulated SPI3 processes during the period from 1 Jan 2009 to 31 Dec 2014. The black boxes in (a)–(c) indicate the 2014 summer and autumn drought in North China, 2011 spring drought in East China, 2009/2010 drought in Southwest China, and 2011 summer drought in Southwest China. Red curves refer to simulated SPI3, while curves filled with light blue represent observed SPI3.

7.3 Drought processes predicted with the CFSv2 forecast datasets

Compared with drought simulation, operationally predicted results may bring some uncertainties into the prospective drought processes. As shown in Fig. 11 (b), predicted curves perform worse than the simulated curves near the peak of the 2011 East China drought, as the prospective observation tendency is rising rather than decreasing. However, in the other three droughts, the predicted curves are well indicating drought development to different degree, resembling the simulated results quite well. For example, the presented operationally reforecast curves indicate drought occurrence, persistence, and relief during the 2009/2010 drought in Southwest China (Fig. 11 (a)).



删除的内容:

删除的内容: 13

删除的内容: 13

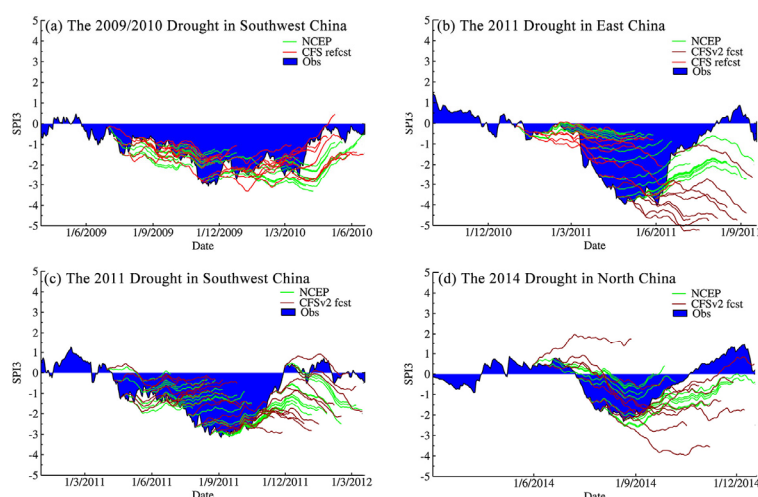


Figure 11. Simulation and prediction results of four recent severe drought events in China. Every unfilled curve represents simulated or predicted prospective 90 day SPI3, with an interval of initial prediction time of about 10 days. The curves filled with blue refer to observed SPI3. Dark and bright red curves refer to SPI3 predicted with CFSv2 and CFS products, respectively. Light green curves represent SPI3 simulated with the NCEP/NCAR reanalysis datasets. Every simulated or predicted curve consists of daily SPI3 time series with 90 points.

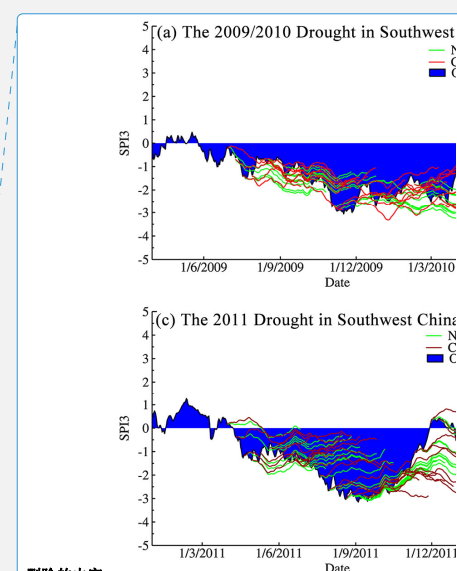
8 Drought outlook

8.1 Angle-based rules

Compared with the predicted prospective SPI3 time series, the drought outlook is a convenient and valuable attachment product for water resource managers. To create the drought outlook, angle-based rules are developed to transform the predicted prospective 90-day SPI3 curves into different drought tendencies. Three essential technical points are as follows.

First, the variables must be defined to describe drought development. Similar to the slope of curves, angles of predicted 90 day SPI3 curves are used to describe the prospective drought situation. Generally, positive angles of SPI3 curves indicate wetter tendencies, while negative angles represent drier tendencies.

The second is two general classifications of drought outlook on the basis of the current drought situation. For no current drought (see sketch map I in Fig. 12), the prospective situation tends to be no drought or drought occurrence. In this case, a critical angle α_1 can be used to help distinguish between these two types of drought outlook. A calculated SPI3 curve angle α that is less than α_1 results in the prospective development of drought occurrence; otherwise, the non-drought situation persists. Similarly, for a current condition of being in drought (see sketch map II in Fig. 12), a comparison of critical angles α_2 (equal



删除的内容:

带格式的: 字体: +西文正文 (Times New Roman)

删除的内容: 14

带格式的: 字体: +西文正文 (Times New Roman)

删除的内容: 14

带格式的: 字体: +西文正文 (Times New Roman)

to zero) and α_3 defines the other three types of drought outlook, which are drought persistence (α less than α_2), drought recession (α more than α_2 , but less than α_3), and drought relief (α more than α_3).

Current drought condition: no drought

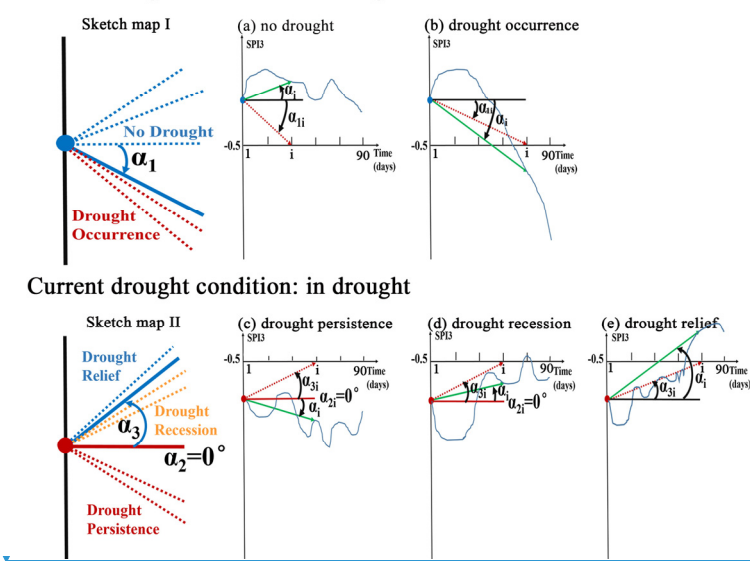
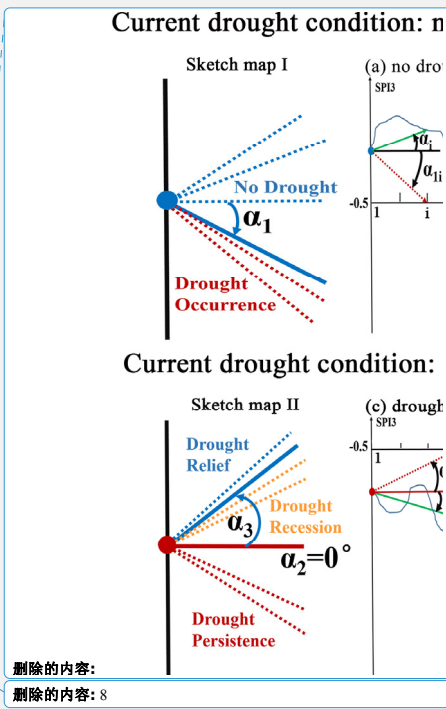


Figure 12. Rules of drought outlook based on angle comparison of prospective 90 day SPI3 curves. Sketch maps I and II show general drought outlook based on current drought situation. (a)–(b) and (c)–(e) express different situations of drought outlook associated with the rules regarding critical angles in Table 7.

Third, it is necessary to explain the practical calculation for curve angles and how to conduct an angle-based drought outlook. Except the constant critical angle α_2 (equal to zero), both α_1 and α_3 represent angles between the horizontal line and arrow from the original point (initial prediction time) to the points on the time axis (see red dashed arrowed lines in Fig. 12(a)–(e)). Similarly, α represents angles between the horizontal line and arrow from the original point to the points on the predicted SPI3 curve (see green solid arrowed lines in Fig. 12(a)–(e)). However, considering the predicted period of SPI3 time series is prospective 90 days, curve angle α_i and critical angles α_{1i} , α_{2i} and α_{3i} ($i=1, 2, \dots, 90$) can be calculated. Finally, according to the angle-based rules shown in Table 7, a drought outlook can eventually be performed.

Table 7. Specific rules for drought outlook based on angle comparison. R1 represents the ratio of days when α_i is less than the critical angle α_{1i} (α_{3i}) to the total 90 days. R2 represents the ratio of specific days in the period of the predicted prospective 46–90 days. In R2 calculation, these specific days meet the criteria that α_i is greater than critical angle α_{3i} .

Current SPI3	Current condition	R1	R2	Drought outlook
greater than -0.5	no drought	less than 10%	-	no drought



删除的内容:

删除的内容: 8

删除的内容: 14

删除的内容: 14

删除的内容: 8

带格式的: 字体颜色: 自动设置

带格式的: 两端对齐, 定义网格后自动调整右缩进, 到齐到网

带格式的: 字体: 加粗, 字体颜色: 自动设置

		greater than 10%	-	drought occurrence
		greater than 90%	less than 90%	drought persistence
less than -0.5	in drought	greater than 90%	greater than 90%	drought recession
		less than 90%	-	drought relief

8.2 Simulated and predicted results

Following the method in Sect. 8.1, drought outlook [js](#) conducted based on angle comparison of the simulated prospective 90-day SPI3 curve (Table [8](#)). Simulations at every initial time are real-time corrected with the current situation. In terms of the 2009/2010 drought in Southwest China and 2011 summer drought in East China, the simulated drought outlook perform well with respect to drought occurrence, persistence, and recession before 2/12/2009 and 1/5/2011 respectively. In addition, the simulation of the 2011 drought in Southwest China performs well in August 2011. The 2014 summer drought in North China lasts for a relatively short time, resulting in an observed drought outlook that maintains a state of drought relief during the first month of the drought process. Even so, the simulation can also capture it. Additionally, these four drought outlooks remain weak in simulating the development of drought relief after 31/1/2010, 11/5/2011, 11/9/2011, and 21/7/2014, respectively. Weak performance in simulating severity leads to the development of drought recession rather than drought relief.

Table 8. Simulation assessment of recent severe drought events in China forced with the NCEP/NCAR Reanalysis datasets. The numbers 0–4 in the below table represent different drought states: no drought (0), drought occurrence (1), drought persistence (2), drought recession (3), and drought relief (4). Besides, the abbreviation “Simul.” and “Obs.” represent the simulated and observed drought outlook, respectively. The abbreviation “Asses.” in the column refers to whether the simulation and observation agree or not.

Drought Events	Initial Time	Simul.	Obs.	Asses.	Initial Time	Simul.	Obs.	Asses.	Initial Time	Simul.	Obs.	Asses.
the 2009/2010 drought in Southwest China	30/6/2009	1	2	-	28/9/2009	3	2	-	11/1/2010	2	3	-
	10/7/2009	2	2	yes	18/10/2009	3	2	-	21/1/2010	2	3	-
	20/7/2009	2	3	-	2/11/2009	3	3	yes	31/1/2010	3	4	-
	30/7/2009	2	3	-	12/11/2009	3	3	yes	10/2/2010	3	4	-
	9/8/2009	2	2	yes	22/11/2009	3	3	yes	20/2/2010	3	4	-
	19/8/2009	2	2	yes	2/12/2009	3	3	yes	2/3/2010	3	4	-
	29/8/2009	2	2	yes	12/12/2009	2	3	-	12/3/2010	3	4	-
	8/9/2009	2	2	yes	22/12/2009	2	3	-	22/3/2010	3	4	-
	18/9/2009	2	2	yes	1/1/2010	2	3	-		-		
the 2011 summer drought in East China	1/1/2011	1	1	yes	2/3/2011	1	1	yes	1/5/2011	3	3	yes
	11/1/2011	1	1	yes	12/3/2011	3	2	-	11/5/2011	3	4	-
	21/1/2011	1	1	yes	22/3/2011	3	2	-	21/5/2011	3	4	-
	31/1/2011	1	1	yes	1/4/2011	3	3	yes	1/6/2011	3	4	-
	10/2/2011	0	1	-	11/4/2011	3	3	yes	11/6/2011	3	4	-
	20/2/2011	1	1	yes	21/4/2011	3	3	yes	21/6/2011	3	4	-
the 2011 summer	11/4/2011	1	1	yes	1/7/2011	3	2	-	21/9/2011	3	4	-
	21/4/2011	2	2	yes	11/7/2011	3	2	-	1/10/2011	3	4	-

删除的内容: calculations are

删除的内容: 9

drought in Southwest China	1/5/2011	2	2	yes	21/7/2011	3	2	-	11/10/2011	3	4	-
	11/5/2011	2	2	yes	1/8/2011	3	3	yes	21/10/2011	3	4	-
	21/5/2011	4	2	-	11/8/2011	3	3	yes	1/11/2011	3	4	-
	1/6/2011	3	2	-	21/8/2011	3	3	yes	11/11/2011	3	4	-
	11/6/2011	3	2	-	1/9/2011	3	3	yes	21/11/2011	2	4	-
	21/6/2011	3	2	-	11/9/2011	3	4	-	-	-	-	-
the 2014 summer drought in North China	1/6/2014	4	4	yes	11/7/2014	3	3	yes	21/8/2014	3	4	-
	11/6/2014	4	4	yes	21/7/2014	3	4	-	1/9/2014	3	4	-
	21/6/2014	4	4	yes	1/8/2014	3	4	-	11/9/2014	3	4	-
	1/7/2014	1	1	yes	11/8/2014	3	4	-	21/9/2014	4	4	yes

415 For predicted drought outlooks, operationally predicted results (Table 9) in Southwest China and East China are relatively similar to the simulated ones (Table 8). In comparison, predicted drought outlook during the first month of the 2014 drought in North China performs worse than simulated results.

Table 9. Same as Table 8 but for predicted results forced with the operational output from CFSv2. The abbreviation “Predi.” represents the predicted drought outlook. The abbreviation “Asses.” in the column refers to whether the prediction and observation agree or not.

Drought Events	Initial Time	Predi.	Obs.	Asses.	Initial Time	Predi.	Obs.	Asses.	Initial Time	Predi.	Obs.	Asses.
the 2009/2010 drought in Southwest China	30/6/2009	1	2	-	28/9/2009	3	2	-	11/1/2010	3	3	yes
	10/7/2009	2	2	yes	18/10/2009	2	2	yes	21/1/2010	3	3	yes
	20/7/2009	3	3	yes	2/11/2009	3	3	yes	31/1/2010	3	4	-
	30/7/2009	3	3	yes	12/11/2009	3	3	yes	10/2/2010	4	4	yes
	9/8/2009	2	2	yes	22/11/2009	3	3	yes	20/2/2010	3	4	-
	19/8/2009	2	2	yes	2/12/2009	3	3	yes	2/3/2010	3	4	-
	29/8/2009	2	2	yes	12/12/2009	3	3	yes	12/3/2010	3	4	-
	8/9/2009	3	2	-	22/12/2009	3	3	yes	22/3/2010	3	4	-
	18/9/2009	2	2	yes	1/1/2010	3	3	yes	-	-	-	-
the 2011 summer drought in East China	1/1/2011	1	1	yes	2/3/2011	1	1	yes	1/5/2011	2	3	-
	11/1/2011	1	1	yes	12/3/2011	2	2	yes	11/5/2011	2	4	-
	21/1/2011	1	1	yes	22/3/2011	2	2	yes	21/5/2011	2	4	-
	31/1/2011	1	1	yes	1/4/2011	2	3	-	1/6/2011	2	4	-
	10/2/2011	1	1	yes	11/4/2011	2	3	-	11/6/2011	3	4	-
	20/2/2011	1	1	yes	21/4/2011	2	3	-	21/6/2011	3	4	-
the 2011 summer drought in Southwest China	11/4/2011	0	1	-	1/7/2011	4	2	-	21/9/2011	3	4	-
	21/4/2011	3	2	-	11/7/2011	3	2	-	1/10/2011	3	4	-
	1/5/2011	3	2	-	21/7/2011	3	2	-	11/10/2011	3	4	-
	11/5/2011	3	2	-	1/8/2011	3	3	yes	21/10/2011	3	4	-
	21/5/2011	4	2	-	11/8/2011	3	3	yes	1/11/2011	3	4	-
	1/6/2011	4	2	-	21/8/2011	3	3	yes	11/11/2011	4	4	yes
	11/6/2011	4	2	-	1/9/2011	3	3	yes	21/11/2011	2	4	-
	21/6/2011	3	2	-	11/9/2011	3	4	-	-	-	-	-

删除的内容: 10

删除的内容: 9

删除的内容: 9

the 2014	1/6/2014	0	4	-	11/7/2014	1	3	-	21/8/2014	3	4	-
summer	11/6/2014	1	4	-	21/7/2014	2	4	-	1/9/2014	4	4	yes
drought in	21/6/2014	1	4	-	1/8/2014	3	4	-	11/9/2014	3	4	-
North	1/7/2014	1	1	yes	11/8/2014	2	4	-	21/9/2014	4	4	yes
China												

9 Discussion

425 Considering that the development of drought processes is closely related to spatio-temporal evolution of atmospheric and
oceanic anomalies, a conceptual prediction model of seasonal drought processes is proposed in our study. Despite its weakness
in predicting drought severity, the model performs well in simulating and predicting drought development. Because the
proposed model is a new attempt, several associated discussion issues are as follows.

First, process prediction and outlook of seasonal drought are the focus of our study. To date, a considerable number of studies
430 have focused on predicting discrete drought classes (Aviles et al., 2016; Bonaccorso et al., 2015; Chen et al., 2013; Moreira et
al., 2016) and the probability of drought occurrence within certain classes (AghaKouchak, 2014, 2015; Hao et al., 2014).
Compared with these studies, process prediction of regional drought events is another valuable attempt, which is beneficial
from the moving window of SPI3 extended from 1 month to 1 day. It performs relatively well in predicting the development
of seasonal drought processes (Fig. 11). In addition, it can indicate drought occurrence, persistence, and relief relatively well
435 (Table 8 and Table 9), which is meaningful for seasonal water resource management.

Second, the proposed model is essentially one stepwise-regression equation, which makes drought prediction for operational
use year-by-year and seamless. Despite its simplicity, it incorporates drought-related spatial and temporal information as
integrally as possible. Because precipitation-related synoptic systems appear in the troposphere, SST, 500 hPa HGT, and 200
hPa HGT are chosen as representatives of the low, middle, upper levels of the troposphere, respectively. Furthermore, all
440 drought process segments assigned to different dry/wet spells are used for EOF analysis within the same dry/wet spells (shown
in Sect. 5.2). Therefore, adequate drought-related spatio-temporal information has been included in these drought predictors.

Third, the reasons for acceptable performance of operationally predicted results need to be illustrated. Compared with those
forced with the NCEP/NCAR Reanalysis datasets (green curves in Fig. 11), the predicted developments of drought processes
forced with CFSv2 or CFS datasets (red curves in Fig. 11) are relatively similar, especially with respect to the former segment
445 of every predicted prospective 90-day SPI3 curve. Essentially, the 90-day-accumulated SA-based predictors strengthen the
good performance of operational use. This indicates that observed information from atmospheric and oceanic anomalies are
involved to different degrees. For instance, the predicted 90-day-accumulated SA-based predictor at the prospective 60th day
is calculated based on a combination of observed data for the past 30 days and dynamically forecasted data for the prospective
1–60 days. With the incorporation of observed data, its operational application provides relatively accurate and valuable
450 information. However, it is also worthwhile to investigate how long the predicted period last can make predicted drought
processes relatively accurate and acceptable, such as the prospective 1–30 day or the prospective 1–60 day. The relevant

带格式的: 字体: +西文正文 (Times New Roman)

删除的内容: 13

带格式的: 字体: +西文正文 (Times New Roman)

删除的内容: 9

带格式的: 字体: +西文正文 (Times New Roman)

删除的内容: 10

带格式的: 字体: +西文正文 (Times New Roman)

删除的内容: 13

带格式的: 字体: +西文正文 (Times New Roman)

删除的内容: 13

带格式的: 字体: +西文正文 (Times New Roman)

comparison results with different predicted periods are shown in Fig. 13. It appears that the 2009/2010 drought in Southwest China and 2014 drought in North China can be predicted and simulated well even for the prospective 1–75 day. In contrast, the prospective 1–45 day may be a feasible and acceptable lead time for simulation and prediction of the 2011 droughts in Southwest China and East China, after which the simulated and predicted developments clearly change.

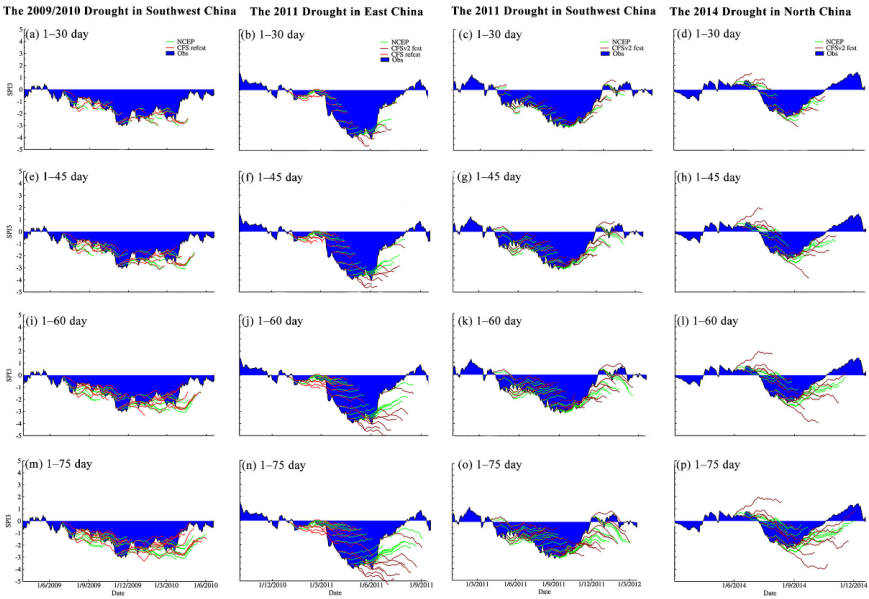


Figure 13. Same as Fig. 11 but for different predicted periods, which are namely the prospective (a)–(d) 1–30 day, (e)–(h) 1–45 day, (i)–(l) 1–60 day, and (m)–(p) 1–75 day.

Fourth, the weak performance in predicting the severity of drought, including drought peak and drought relief, is an important issue. Similar to the concluding remarks regarding a probabilistic drought prediction model, the weak performance in predicting the severity of the drought peak is due to the typical problem of an inherent averaging effect depressing the extremes (Behrangi et al., 2015). With the help of real-time correction for operational application, the prediction of drought peaks can be improved. In addition, the prediction of drought relief should also be considered. As listed in both Table 8 and Table 9, the simulated and predicted results for drought relief are unsatisfying. This weak performance may be associated with precipitation-causing weather patterns during drought relief. They are unsteady and change dramatically compared with those features during drought persistence. Because the period of drought relief is a relatively short phase of the drought process, the relevant information may not be involved in the first EOF modes (Sect. 5.2). Generally, three measures for potential improvement are as follows. (1) More secondary EOF modes, including precipitation-causing circulation patterns during

删除的内容: 15
带格式的: 字体: +西文正文 (Times New Roman)

删除的内容: 13

删除的内容: 9
删除的内容: 10

drought relief, can be incorporated when building initial predictors. (2) The rapid change index (Otkin et al., 2015) could be introduced to describe temporal changes during drought relief at sub-seasonal time scales. (3) The empirical factor can be introduced to improve drought-relief prediction. The predicted SPI3 during the phase of drought relief could be multiplied by empirical factors to strengthen drought relief development.

Fifth, it is necessary to explain the method of predictor construction. The predictor-structured method in our study is similar to the definition of tele-connection indices (Wallace and Gutzler, 1981). It is more goal-directed, because these structured predictors are directly related to synchronous atmospheric/oceanic anomalous circulation patterns during different drought segments within the same dry/wet spells. However, to design geographical ranges of anomalous areas and combine them is subjective, which leads to considerable uncertainties. Accordingly, an objective anomaly-recognized method with explicit critical values needs to be developed. This will contribute to auto-run feasibility of this conceptual prediction model without artificial interaction.

The final issue to illustrate is synchronous SST anomalies used in EOF analysis and model construction. Traditionally, SST anomalies a few months ahead influence the subsequent regional drought. However, it is also feasible and common that synchronous SST anomalies are used in the investigation of regional drought events in Southwest China (Feng et al., 2014), the Yangtze River basin (Lu et al., 2014), and North China (Wang and He, 2015), which may shape synchronous drought-related circulation patterns. In addition, this is convenient for operational application, while forecasted SST and 200 hPa / 500 hPa HGT can be retrieved together from CFSv2 products simultaneously.

10 Conclusions

Drought prediction is fundamental for seasonal water management. In this study, we constructed a conceptual prediction model of seasonal drought processes based on synchronous Standardized Anomalies (SA) of 200 hPa/500 hPa geo-potential height (HGT) and sea surface temperature (SST); we considered that drought development is closely related to the spatio-temporal evolution of large-scale atmospheric/oceanic circulation patterns. We used North China as an example to introduce the method and used four recent severe regional drought events in China for application. This model can be used for seamless drought prediction and drought outlook, forced with seasonal climate forecast models. The main process is as follows. (1) 3-month SPI updated daily (SPI3) was used to capture severe and extreme drought processes. (2) Empirical Orthogonal Function (EOF) analysis was applied to SA of 200 hPa/500 hPa HGT and SST during drought process segments within the same dry/wet spells. Subsequently, spatial patterns of the first EOF modes were used to structure SA-based predictors. (3) The synchronous stepwise-regression relationship between SPI3 and all 90-day-accumulated SA-based predictors were calibrated using the NCEP/NCAR reanalysis datasets. (4) To achieve prospective 90-day drought outlook, we further developed an objective method based on angles of the predicted prospective 90-day SPI3 curves. (5) Finally, simulation and prediction of seasonal drought processes, together with drought outlook, were forced with the NCEP/NCAR reanalysis datasets and the NCEP Climate Forecast System Version 2 (CFSv2) operationally forecasted datasets, respectively. Model application during four

删除的内容: prediction

recent severe drought events in China revealed that the model is good at development prediction but weak in severity prediction. These results indicate that the proposed conceptual drought prediction model is another potentially valuable addition to current research on drought prediction.

Acknowledgements

515 This work is supported by the Special Public Sector Research Program of Ministry of Water Resources (Grants No. 201301040 and 201501041), Fundamental Research Funds for the Central Universities (Grant No. 2015B20414), Program for New Century Excellent Talents in University (Grant No. NCET-12-0842), National Natural Science Foundation of China (Grant No. 51579065), and Natural Science Foundation of Jiangsu Province of China (Grant No. BK20131368). In addition, we are grateful for the editor and the two anonymous referees. Their comments and suggestions help improve the clarity of the manuscript and make us think about the research work more deeply.

Competing interests

The authors declare that they have no conflict of interest.

References

525 Afifi, A. A., and Azen, S. P.: Statistical analysis: a computer oriented approach, Academic press, 1972.
AghaKouchak, A.: A baseline probabilistic drought forecasting framework using standardized soil moisture index: application to the 2012 United States drought, Hydrology and Earth System Sciences, 18, 2485-2492, 10.5194/hess-18-2485-2014, 2014.
530 AghaKouchak, A.: A multivariate approach for persistence-based drought prediction: Application to the 2010-2011 East Africa drought, Journal of Hydrology, 526, 127-135, 10.1016/j.jhydrol.2014.09.063, 2015.
Aviles, A., Celleri, R., Paredes, J., and Solera, A.: Evaluation of Markov Chain Based Drought Forecasts in an Andean Regulated River Basin Using the Skill Scores RPS and GMSS, Water Resources Management, 29, 1949-1963, 10.1007/s11269-015-0921-2, 2015.
535 Aviles, A., Celleri, R., Solera, A., and Paredes, J.: Probabilistic Forecasting of Drought Events Using Markov Chain- and Bayesian Network-Based Models: A Case Study of an Andean Regulated River Basin, Water, 8, 16, 2016.
Behrangi, A., Hai, N., and Granger, S.: Probabilistic Seasonal Prediction of Meteorological Drought Using the Bootstrap and Multivariate Information, Journal of Applied Meteorology and Climatology, 54, 1510-1522, 10.1175/jamc-d-14-0162.1, 2015.
Belayneh, A., Adamowski, J., Khalil, B., and Ozga-Zielinski, B.: Long-term SPI drought forecasting in the Awash River Basin in Ethiopia using wavelet neural network and wavelet support vector regression models, Journal of Hydrology, 508, 418-429, 10.1016/j.jhydrol.2013.10.052, 2014.
540 Bonaccorso, B., Cancelliere, A., and Rossi, G.: Probabilistic forecasting of drought class transitions in Sicily (Italy) using Standardized Precipitation Index and North Atlantic Oscillation Index, Journal of Hydrology, 526, 136-150, 10.1016/j.jhydrol.2015.01.070, 2015.
Chen, S. T., Yang, T. C., Kuo, C. M., Kuo, C. H., and Yu, P. S.: Probabilistic Drought Forecasting in Southern Taiwan Using El-Nino-Southern Oscillation Index, Terr Atmos Ocean Sci, 24, 911-924, 2013.
545

删除的内容: Nirio

Dai, A. G.: Drought under global warming: a review, *Wires Clim Change*, 2, 45-65, 2011.

Duan, W. L., He, B., Takara, K., Luo, P. P., Nover, D., Yamashiki, Y., and Huang, W. R.: Anomalous atmospheric events leading to Kyushu's flash floods, July 11-14, 2012, *Nat. Hazards*, 73, 1255-1267, 2014.

550 Dutra, E., Di Giuseppe, F., Wetterhall, F., and Pappenberger, F.: Seasonal forecasts of droughts in African basins using the Standardized Precipitation Index, *Hydrology and Earth System Sciences*, 17, 2359-2373, 10.5194/hess-17-2359-2013, 2013.

Dutra, E., Pozzi, W., Wetterhall, F., Di Giuseppe, F., Magnusson, L., Naumann, G., Barbosa, P., Vogt, J., and Pappenberger, F.: Global meteorological drought - Part 2: Seasonal forecasts, *Hydrology and Earth System Sciences*, 18, 2669-2678, 2014.

Feng, L., Li, T., and Yu, W.: Cause of severe droughts in Southwest China during 1951-2010, *Climate Dyn.*, 43, 2033-2042, 10.1007/s00382-013-2026-z, 2014.

555 Funk, C.: We thought trouble was coming, *Nature*, 476, 7-7, 2011.

Funk, C., Hoell, A., Shukla, S., Blade, I., Liebmann, B., Roberts, J. B., Robertson, F. R., and Husak, G.: Predicting East African spring droughts using Pacific and Indian Ocean sea surface temperature indices, *Hydrology and Earth System Sciences*, 18, 4965-4978, 10.5194/hess-18-4965-2014, 2014.

560 Grumm, R. H., and Hart, R.: Standardized anomalies applied to significant cold season weather events: Preliminary findings, *Wea. Forecasting*, 16, 736-754, 10.1175/1520-0434(2001)016<0736:saatsc>2.0.co;2, 2001.

Hart, R. E., and Grumm, R. H.: Using normalized climatological anomalies to rank synoptic-scale events objectively, *Mon. Wea. Rev.*, 129, 2426-2442, 10.1175/1520-0493(2001)129<2426:uncatr>2.0.co;2, 2001.

Hurrell, J. W.: Decadal trends in the north Atlantic oscillation: regional temperatures and precipitation, *Science (New York, N.Y.)*, 269, 676-679, 10.1126/science.269.5224.676, 1995.

565 Jiang, N., Qian, W. H., Du, J., Grumm, R. H., and Fu, J. L.: A comprehensive approach from the raw and normalized anomalies to the analysis and prediction of the Beijing extreme rainfall on July 21, 2012, *Nat. Hazards*, 84, 1551-1567, 10.1007/s11069-016-2500-0, 2016.

Kalnay, E., Kanamitsu, M., Kistler, R., Collins, W., Deaven, D., Gandin, L., Iredell, M., Saha, S., White, G., Woollen, J., Zhu, Y., Chelliah, M., Ebisuzaki, W., Higgins, W., Janowiak, J., Mo, K. C., Ropelewski, C., Wang, J., Leetmaa, A., Reynolds, R., Jenne, R., and Joseph, D.: The NCEP/NCAR 40-year reanalysis project, *Bulletin of the American Meteorological Society*, 77, 437-471, 10.1175/1520-0477(1996)077<0437:tnyrp>2.0.co;2, 1996.

570 Kingston, D. G., Stagge, J. H., Tallaksen, L. M., and Hannah, D. M.: European-Scale Drought: Understanding Connections between Atmospheric Circulation and Meteorological Drought Indices, *Journal of Climate*, 28, 505-516, 10.1175/jcli-d-14-00001.1, 2015.

575 Lu, E., Liu, S. Y., Luo, Y. L., Zhao, W., Li, H., Chen, H. X., Zeng, Y. T., Liu, P., Wang, X. M., Higgins, R. W., and Halpert, M. S.: The atmospheric anomalies associated with the drought over the Yangtze River basin during spring 2011, *J Geophys Res-Atmos*, 119, 5881-5894, 2014.

McKee, T. B. D., N.J., and Kleist, J.: The relationship of drought frequency and duration to time scales, 8th Conference on Applied Climatology, Anaheim, Calif., 1993.

580 Mehr, A. D., Kahya, E., and Ozger, M.: A gene-wavelet model for long lead time drought forecasting, *Journal of Hydrology*, 517, 691-699, 10.1016/j.jhydrol.2014.06.012, 2014.

Mishra, A. K., and Singh, V. P.: Drought modeling - A review, *Journal of Hydrology*, 403, 157-175, 2011.

585 Mo, K. C., and Lyon, B.: Global Meteorological Drought Prediction Using the North American Multi-Model Ensemble, *Journal of Hydrometeorology*, 16, 1409-1424, 2015.

Moreira, E. E., Pires, C. L., and Pereira, L. S.: SPI Drought Class Predictions Driven by the North Atlantic Oscillation Index Using Log-Linear Modeling, *Water*, 8, 18, 2016.

Otkin, J. A., Anderson, M. C., Hain, C., and Svoboda, M.: Using Temporal Changes in Drought Indices to Generate Probabilistic Drought Intensification Forecasts, *Journal of Hydrometeorology*, 16, 88-105, 10.1175/jhm-d-14-0064.1, 2015.

590 Reynolds, R. W., Smith, T. M., Liu, C., Chelton, D. B., Casey, K. S., and Schlax, M. G.: Daily high-resolution-blended analyses for sea surface temperature, *Journal of Climate*, 20, 5473-5496, 10.1175/2007jcli1824.1, 2007.

Rong, Y., Duan, L., and Xu, M.: Analysis on Climatic Diagnosis of Persistent Drought in North China during the Period from 1997 to 2002, *Arid Zone Research*, 25, 842-850, 2008.

595 Ropelewski, C. F., and Halpert, M. S.: Global and Regional Scale Precipitation Patterns Associated with the El Niño/Southern Oscillation, *Monthly Weather Review*, 115, 1606-1626, doi:10.1175/1520-0493(1987)115<1606:GARSPP>2.0.CO;2, 1987.

- Saha, S., Moorthi, S., Wu, X. R., Wang, J., Nadiga, S., Tripp, P., Behringer, D., Hou, Y. T., Chuang, H. Y., Iredell, M., Ek, M., Meng, J., Yang, R. Q., Mendez, M. P., Van Den Dool, H., Zhang, Q., Wang, W. Q., Chen, M. Y., and Becker, E.: The NCEP Climate Forecast System Version 2, *Journal of Climate*, 27, 2185-2208, 2014.
- Shin, J. Y., Ajmal, M., Yoo, J., and Kim, T.-W.: A Bayesian Network-Based Probabilistic Framework for Drought Forecasting and Outlook, *Advances in Meteorology*, 10.1155/2016/9472605, 2016.
- Wallace, J. M., and Gutzler, D. S.: Teleconnections in the Geopotential Height Field during the Northern Hemisphere Winter, *Mon. Wea. Rev.*, 109, 784-812, 1981.
- Wang, H. J., and He, S. P.: The North China/Northeastern Asia Severe Summer Drought in 2014, *Journal of Climate*, 28, 6667-6681, 2015.
- Wei, J., Zhang, Q., and Tao, S.: Physical Causes of the 1999 and 2000 Summer Severe Drought in North China, *Chinese Journal of Atmospheric Sciences*, 28, 125-137, 2004.
- Wilks, D. S.: Principal Component (EOF) Analysis, in: *Statistical methods in the atmospheric sciences*, Academic press, 519-562, 2011.
- World Meteorological Organization. Standardized Precipitation Index User Guide; WMO: Geneva, Switzerland, 2012.
- Available online: http://www.wamis.org/agm/pubs/SPI/WMO_1090_EN.pdf (accessed on 7 June 2017)
- Wood, E. F., Schubert, S. D., Wood, A. W., Peters-Lidard, C. D., Mo, K. C., Mariotti, A., and Pulwarty, R. S.: Prospects for Advancing Drought Understanding, Monitoring, and Prediction, *Journal of Hydrometeorology*, 16, 1636-1657, 2015.
- Yang, J., Gong, D. Y., Wang, W. S., Hu, M., and Mao, R.: Extreme drought event of 2009/2010 over southwestern China, *Meteorol Atmos Phys*, 115, 173-184, 2012.
- Yoon, J. H., Mo, K., and Wood, E. F.: Dynamic-Model-Based Seasonal Prediction of Meteorological Drought over the Contiguous United States, *Journal of Hydrometeorology*, 13, 463-482, 2012.
- Yuan, X., Wood, E. F., Roundy, J. K., and Pan, M.: CFSv2-Based Seasonal Hydroclimatic Forecasts over the Conterminous United States, *Journal of Climate*, 26, 4828-4847, 2013.

8, but for Standardized Anomalies (SA) of 200 hPa geo-potential height fields (HGT).

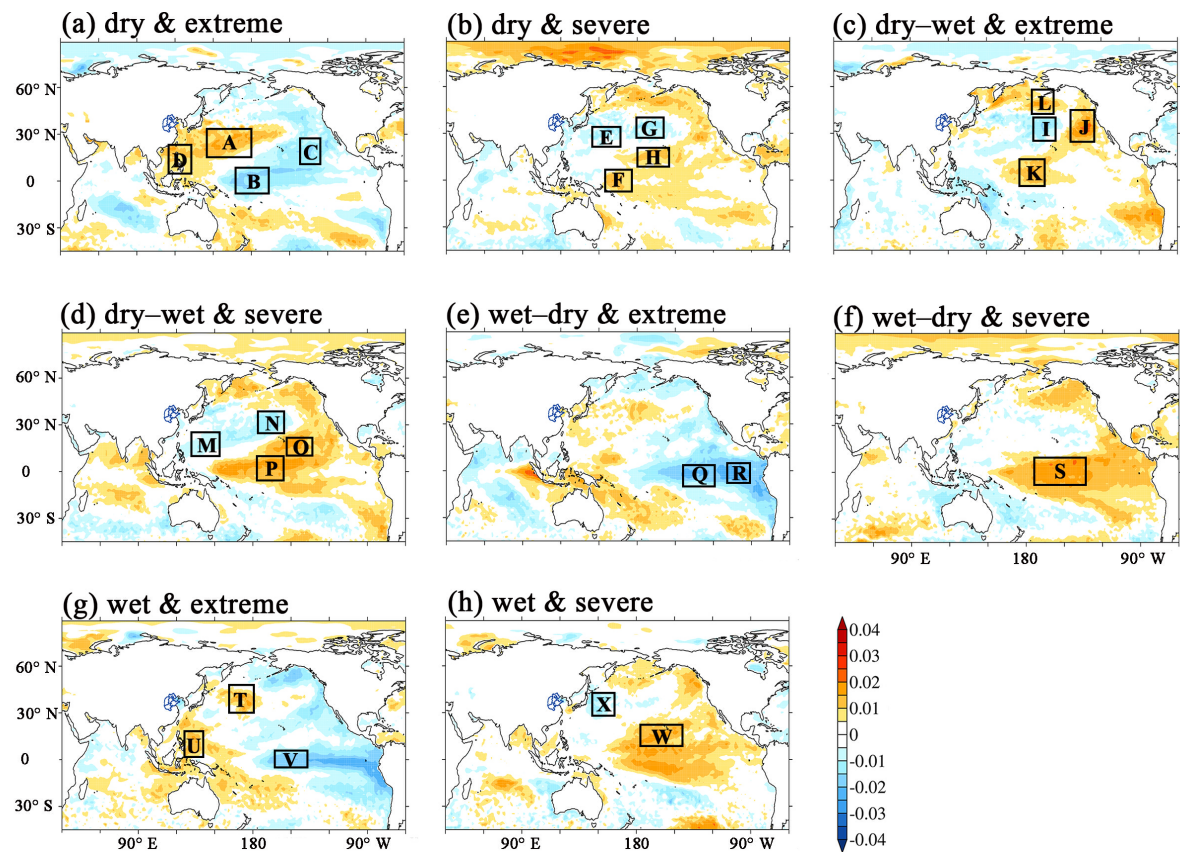


Figure 10. Same as Fig. 8

Table 7. List of the selected predictors and relevant coefficients during different calibration periods in North China. Types and codes correspond to Table 5.

Type	Code	Calibration period (1983–)					
		2008	2009	2010	2011	2012	2013
SST	0	0.003	0.003	0.003	0.003	0.003	0.001
	1	-0.005	-0.004	-0.004	-0.003	-0.003	-0.002
	2	0.002	0.003	0.003	0.002	0.002	0.003
	3	0.002	0.003	0.002	0.002	0.002	0.002
	4	-0.005	-0.005	-0.005	-0.005	-0.005	-0.004
	5	-	-	0.000	0.001	0.001	-
	6	-0.001	0.000	-0.001	-0.001	-0.001	-
	7	-0.001	-0.001	-0.002	-0.002	-0.001	-
	8	-0.003	-0.003	-0.003	-0.003	-0.003	-0.003
	9	0.003	0.004	0.006	0.004	0.003	0.002
	10	0.001	0.001	0.001	0.001	0.001	0.000

	11	-	-	-0.002	-0.001	-	-
	12	-0.002	-0.001	-0.001	-0.001	0.000	-0.001
	13	0.003	0.003	0.003	0.003	0.003	-
	14	0.003	0.003	0.003	0.003	0.003	0.003
200 hPa HGT	0	-	-	-	-	-	-0.001
	1	0.003	0.002	0.003	0.003	0.003	0.002
	2	0.015	0.013	0.015	0.015	0.015	0.015
	3	-0.003	-	-0.002	-0.003	-0.003	-0.003
	4	-0.001	-	-	-	-	-
	5	0.009	0.008	0.008	0.008	0.008	0.008
	6	-0.003	-0.004	-0.003	-0.003	-0.004	-0.003
	7	0.015	0.013	0.014	0.014	0.014	0.014
	8	-0.008	-0.007	-0.007	-0.007	-0.006	-0.006
	9	0.005	0.004	0.004	0.004	0.005	0.005
	10	0.009	0.009	0.008	0.008	0.008	0.009
	11	-	-0.002	-	-	-	-
	12	0.003	0.003	0.003	0.003	0.002	0.001
	13	-0.004	-0.003	-0.004	-0.004	-0.004	-0.004
500 hPa HGT	0	-0.002	-0.002	-0.002	-0.002	-0.002	-0.002
	1	-0.009	-0.008	-0.008	-0.008	-0.008	-0.008
	2	-	-	-	-	-	0.003
	3	0.007	0.007	0.007	0.007	0.007	0.005
	4	0.014	0.013	0.012	0.012	0.012	0.009
	5	-0.004	-0.003	-0.003	-0.003	-0.003	-0.002
	6	0.016	0.015	0.016	0.016	0.016	0.013
	7	-0.018	-0.017	-0.018	-0.017	-0.017	-0.014
	8	-0.018	-0.018	-0.018	-0.017	-0.018	-0.018
	9	0.009	0.009	0.009	0.008	0.008	0.008
	10	-0.010	-0.010	-0.010	-0.009	-0.010	-0.010
	11	-0.005	-0.005	-0.005	-0.005	-0.005	-0.005
	12	-0.016	-0.014	-0.015	-0.014	-0.015	-0.013
	13	-0.011	-0.012	-0.011	-0.011	-0.010	-0.010